J Electroceram (2010) 24:170–176
DOI 10.1007/s10832-008-9553-8

Dielectric and piezoelectric properties of PZT ceramics with anisotropic porosity

D. Piazza · C. Galassi · A. Barzegar · D. Damjanovic

Received: 23 July 2008 / Accepted: 22 September 2008 / Published online: 8 October 2008

Abstract $Pb(Zr,Ti)O_3$ ceramics with homogenous, anisotropic porosity were manufactured and the influence of the anisotropic porosity on the dielectric and piezoelectric properties was studied. Image analysis allowed the quantification of the preferential orientation and the calculation of the distribution of the aspect ratio of the pores. The different dependence of the permittivities ε_{33}^T and ε_{11}^T on the porosity content demonstrates that the population of pores is constituted of a high volume of pores with low aspect ratio and a low volume of pores with high aspect ratio. In view of the quantitative results obtained on the microstructure, an explanation of the frequency dependence of the dielectric and piezoelectric behaviour is suggested. Furthermore, the higher d_{31} piezoelectric coefficient in the material with anisotropic pores than in material with isotropic pores is related to higher effective fields which are a consequence of the enhanced longitudinal mobility of the material under transverse stress.

Keywords Anisotropic porosity · Image analysis · Dielectric spectroscopy · PZT

D. Piazza · C. Galassi (✉)
Istituto di Scienza e Tecnologia dei Materiali Ceramici—Consiglio Nazionale delle Ricerche, ISTEC-CNR Via Granarolo 64, 48018 Faenza, RA, Italy
e-mail: carmen.galassi@istec.cnr.it

A. Barzegar · D. Damjanovic
Ceramics Laboratory, Materials Department, Swiss Federal Institute of Technology-EPFL, 1015 Lausanne, Switzerland

1 Introduction

Piezoelectric ceramics are widely used materials in actuators, ultrasonic transducers and transformers [1]. Their employment in such different applications requires optimization of specific performance parameters. As reported elsewhere [2–4] the application of porous materials in acoustic application is gaining in importance. One of the applications is in hydrophones where they work as acoustic transducers. As hydrophones are mostly operated at low frequencies (<100 kHz), the external stress can be considered hydrostatic [5]. The performance in terms of sensitivity can be expressed as a figure of merit $FOM=d_h g_h$ with $d_h = d_{33} + 2d_{31}$ and $g_h = g_{33} + 2g_{31}$. Dense $Pb(Zr,Ti)O_3$ (PZT) ceramics show a very low FOM since $d_{33} \approx 2d_{31}$ and $g_{33} \approx 2g_{31}$. The FOM can be enhanced by orders of magnitude by employing composite materials with very low d_{31} and g_{31} and with relatively high g_{33}. In fact composite polymer–ceramic materials [6] with 1–3 and 2–2 connectivity, as defined by Newnham et al. [7], are widely used in hydrophones and medical imaging transducers. Most of the methods for making piezoelectric composites are complex, time consuming and costly [8]. By adding pore forming agents [9] to the ceramic powder followed by burning of the organics, a "composite" ceramic–air material is produced through a cheap ceramic process, but with performance comparable to the cut and fill 3–3 composite. The porosity reflects on the performance either by the purely electromechanical effect of removing piezoelectric and highly dielectric material, or with a more complicated effect on the domain walls and polarization dynamics [10].

The volume, size and aspect ratio (which is the ratio between major and minor axis of the pore assumed to be pseudo-elliptic) of the voids are critical parameters that must be controlled in order to optimize the performance of

the porous ceramics. If the pore volume is kept constant, the effective dielectric permittivity of the material will have two limiting behaviours, determined by the ferroelectric phase being parallel or in series with the pores. As shown in [11], for low amount of porosity the difference between the two cases is tremendous and is relevant even at higher porosity content. Similar effects are noticeable for the mechanical and piezoelectric properties of porous materials. This determines the necessity to find appropriate tools to analyse the structure of the porosity.

One approach used [12] is to simulate the microstructure and the piezoelectric response of the porous material with the finite element method and to validate the proposed microstructure by comparing the results obtained with the experimental ones. The quantitative study of the microstructures has been used mainly for the analysis of the mechanical properties of ceramic materials [13, 14]. On the other side, in spite of a large amount of literature on porous piezoelectric ceramics, it seems that a correlation of the pore morphology data from the viewpoint of the statistical analysis, with the dielectric and piezoelectric properties is not available.

In this perspective, the aim of this work is to perform a quantitative analysis of the preferential alignment of the porosity of PZT composites with pores filled with air as the second, piezoelectrically inactive phase and to correlate the microstructural features with the piezoelectric and dielectric response.

2 Experimental

2.1 Sample preparation

Powders of the composition $Pb_{0.988}(Zr_{0.52}\ Ti_{0.48})_{0.976}Nb_{0.024}O_3$ were prepared following the mixed-oxide method. In order to prepare the porous samples different amounts (5, 10, 20, 40 vol.%) of fine graphite were mixed to the PZT powders and disk samples with 2 mm thickness and 25 mm diameter were produced from each mixture by die pressing. Cylinders with diameter 5.3 mm and thickness 2.5 mm of dense ceramics and ceramics containing 38 vol.% of porosity were also produced by die pressing. All samples were sintered at 1150°C for 2 h at heating rate of 100°C/h to let the complete burning of graphite. In order to avoid the loss of PbO, the sintering of all samples was carried out in a sealed Al_2O_3 crucible with the samples placed on ZrO_2 disks next to $PbZrO_3$+5 wt.% excess ZrO_2 powder. The reproducibility of the process was controlled by producing 20 samples with 40 vol.% of graphite. The variation of the d_{33}, g_{33}, and ε_{33}, of examined samples was 26%, 6% and 20% respectively. The further analysis was performed on one representative sample of each group.

The sintered samples show porosity values ranging from 5 to 38 vol.% [details are reported in [15]. From the mercury intrusion porosimetry analysis it was found that the porosity is mostly open and tridimensionally interconnected (e.g., 32 vol.% open porosity out of 38 vol.% total porosity in the sample with 40 vol.% graphite).

2.2 Image analysis

Micrographs of the microstructure were obtained by Scanning Electron Microscopy (SEM) (Cambridge Inca Oxford Instruments) on as polished samples. Quantitative analysis of the microstructure of the porous samples was done on micrographs obtained by SEM analysis on faces parallel to the direction of applied pressure during cold consolidation (Fig. 1); the image is shown with the abscissa in the direction of the applied pressure and the ordinate is taken in the image analysis as the vertical. The images were analyzed through Image Pro Plus 4.5 and Matlab 7 to determine the pore aspect ratio and preferential angle with the vertical axis. The digital images acquired were highly contrasted in order to evidence the pores and to reduce the intrinsic uncertainty in pore recognition with a size of 2,037×1,709 pixels. With the software Image Pro Plus, the pores were separated from the background, setting the separation at channel 250 out of 255 channels. The software recognizes pores as the objects constituted by pixels which are contiguous to each other. All the objects found were then separated based on their size, and those with an area smaller than 10 μm^2 were not considered in the further analysis. This threshold size was chosen in order to cut out small defects coming from the polishing procedure and the

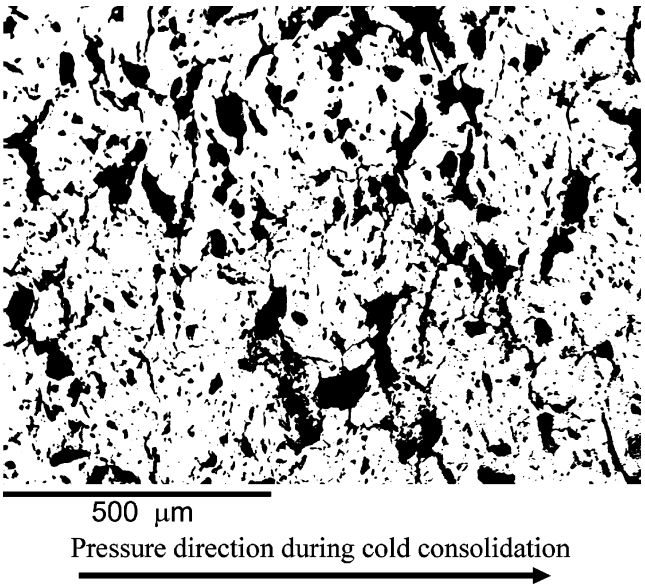

Fig. 1 BSE SEM image on surface parallel to the direction of applied pressure during cold consolidation

small porosity (about 5 vol.% with mean size around 3–4 μm) that is residual from the primary particle's packing and originates in the fact that the densification conditions were not enough to reach full density of the pore walls. This cut off procedure does not allow the comparison of the total porosity found with the SEM micrographs with porosimeter analysis, but does ensure the possibility of studying the aspect ratio and preferential orientation of the macro pores in a semi quantitative manner; 2008 pores were considered in four images to analyze the reproducibility. The data were then analyzed in Matlab 7 in order to study the statistical distribution of the results.

2.2.1 Piezo-dielectric characterization

In order to measure the anisotropy of the ε_{ii}^{T}, unpoled samples were cut and electroded either (a) parallel to the direction of the applied pressure during cold consolidation (direction 3, to determine ε_{33}^{T}) or (b) perpendicular to the applied pressure (direction 1, to determine ε_{11}^{T}). The capacitance of the samples was determined using an impedance/gain phase analyzer HP4194A at the frequency of 1 kHz and voltage of 0.5 V.

Measurements of the direct piezoelectric effect as a function of frequency were obtained using a dynamic press system described in detail in [14]. Dielectric spectroscopy at very low frequencies (0.01–100 Hz) was carried out with a Stanford Research SR830 DSP lock-in amplifier and Kistler 5011 charge amplifier.

3 Results and discussion

3.1 Microstructure analysis

The microstructure developed by introducing graphite as the pore forming agent is anisotropic even at low graphite content, as reported in [15]. In the present work, the image analysis is focused on the samples with 38 vol.% of porosity. The microstructure of these samples is highly anisotropic with the presence of few cracks, as shown by SEM micrographs (Fig. 1). In the semi-quantitative analysis, the pores are assumed to be pseudo-elliptical, allowing the definition of the aspect ratio and of the angle of the major axis with respect to the vertical of the images, i.e. perpendicularly to the direction of applied pressure. The distribution of the angles of the pores between the major axis and the vertical of the images is fitted with a normal distribution centred at zero, with a high variance (μ=0°, σ=43°) and is reported in Fig. 2. The analysis shows that the pores are preferentially aligned with the major axis perpendicular to the direction of the applied pressure, which is defined by 0°. On the other side, the high variance

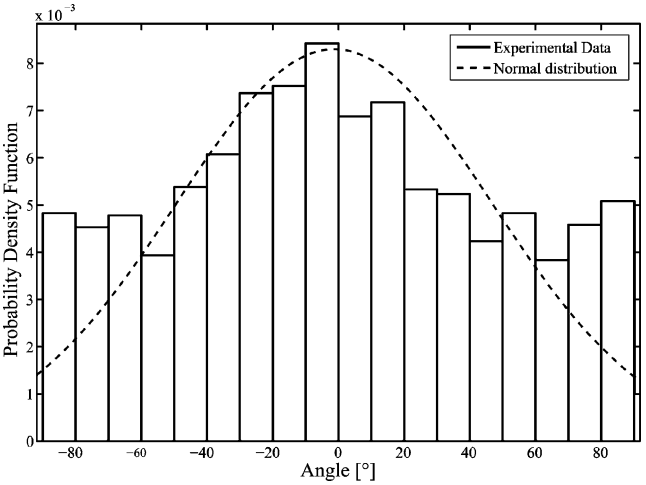

Fig. 2 Experimental results and Probability Density Function for the Normal distribution of angles of major axis of the pores with respect to the perpendicular to the direction of applied pressure during cold consolidation

indicates that a distribution of randomly aligned pores is convoluted with the distribution of aligned pores.

As reported in Fig. 3, the data for the aspect ratio were better fitted by the Birnbaum–Saunders distribution [16] first developed in studies for life tests of steel specimens subjected to fatigue treatment, with the following density function:

$$\frac{1}{\sqrt{2\pi}}\exp\left\{-\frac{\left(\sqrt{x/\beta}-\sqrt{\beta/x}\right)^2}{2\gamma^2}\right\}\left(\frac{\sqrt{x/\beta}+\sqrt{\beta/x}}{2\gamma x}\right) \tag{1}$$

where β=2.22 and γ=0.42 are shape parameters and the mean and variance are 2.42 and 1.1 respectively.

The χ^2 test with five degrees of freedom shows very good agreement of this distribution with the experimental data (χ^2=0.678), taking into account that the aspect ratio z is

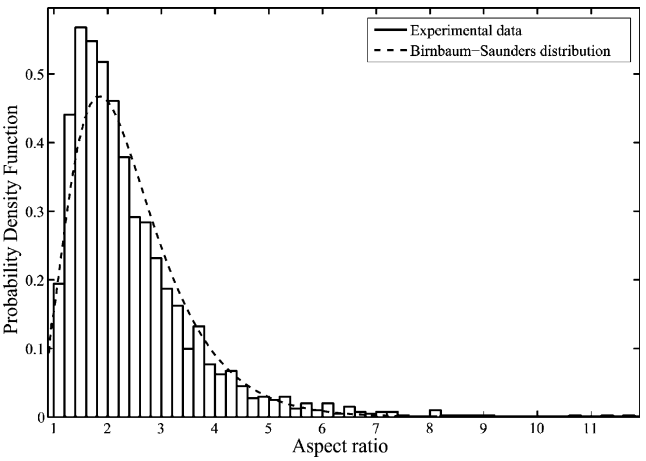

Fig. 3 Experimental results and Probability Density Function for Birnbaum–Saunders distribution of the aspect ratio of the pores

defined only for $x \geq 1$. On the other side, the Birnbaum–Saunders distribution associates nonzero probabilities to these values as well (the Birnbaum–Saunders distribution is defined for values <1 while the aspect ratio is not. Anyway the probability density associated to value less then 1 is only around 4% and the very good results of the χ^2 test make this compromise acceptable). It should be noticed that the χ^2 test also displays slightly inferior results for a log-normal distribution, that is generally used in describing anisotropic microstructure [13]. For this reason it was decided to apply this distribution that was derived from a model that worked well to correlate the material failure to the development and growth of a dominant crack. Even though we are dealing with a microstructure with anisotropic grains and cracks, and from an empirical stand point it is observed that the distribution fits the data quite well, a deeper study of the physical subsistence of the use of this distribution is necessary to demonstrate that this is the limit distribution of the aspect ratio of pores.

The reproducibility of the results is quite good. In fact, the mean and the standard deviation of the normal distribution of the mean of the Birnbaum–Saunders distributions of the pore aspect ratio in four different micrographs is μ=2.42, with variance =0.003. The same distribution applied to objects with an area wider than 3,000 μm^2 shows a decrease of the mean of more than 5%. By analyzing the data of preferential angle and aspect ratio, a general correlation with the area of the pores can be drawn which indicates that the distribution of the pores is the convolution of: (a) big pores with area larger than 3,000 μm^2 with low aspect ratio, (b) medium sized pores with area between 3,000 μm^2 and 50 μm^2 with higher mean aspect ratio and preferentially aligned perpendicularly to the direction of applied pressure, and (c) randomly aligned small sized pores with high mean aspect ratio.

3.2 Dielectric permittivity at 1 kHz

The pores can be considered as a secondary phase with a dielectric permittivity close to that of vacuum. Studying ε_{33}^T and ε_{11}^T of the composite, a quantitative evaluation of the mean electrical circuit associated to this microstructure can be obtained, assuming that at the frequency of 1 kHz the relaxation effects are negligible [17–29]. The complexity of the microstructure is confirmed by the anisotropy of the dielectric constant of unpoled samples. The values of ε_{33}^T and ε_{11}^T decrease at increasing pore volume, but following a different trend as reported in Fig. 4.

In fact the ε_{33}^T variation with the pore content follows the modified 3–3 model for composites with open pores [30] quite well:

$$\frac{\varepsilon_{33c}^T}{\varepsilon_0} = \frac{\varepsilon_{33m}^T}{\varepsilon_0}\left[(1-a)^2 + 2a(1-a)(1-r)\right] \tag{2}$$

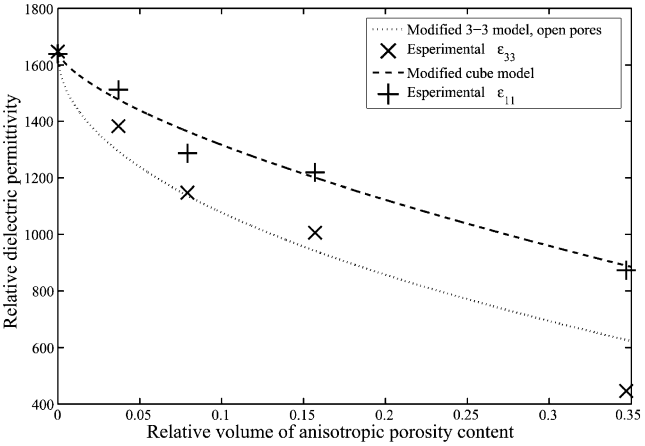

Fig. 4 Relative dielectric permittivity at different direction and porosity content

where ε_{33c}^T is the dielectric permittivity of the porous material, ε_{33m}^T is the dielectric permittivity of the bulk ceramic, r=0.5 (corresponding to an aspect ratio of 2) is the anisotropy factor and the parameter a can be obtained by:

$$p = a^3 + 3a^2(1-a)r^2 \tag{3}$$

where p is the porosity.

On the other side, the data for ε_{11}^T agree better with a modified cube model [31] (associated to a 3–0 composite, i.e., closed porosity):

$$\frac{\varepsilon_{11c}^T}{\varepsilon_0} = \frac{\varepsilon_{11m}^T}{\varepsilon_0}\left\{1 + \frac{a^2}{K_s^{2/3}}\frac{1}{a\left(\frac{\varepsilon_{11m}^T}{\varepsilon_0}-1\right)K_s^{2/3}+1} - \frac{a^2}{K_s^{2/3}}\right\} \tag{4}$$

where ε_{11c}^T is the dielectric permittivity of the porous material, ε_{11m}^T is the dielectric permittivity of the bulk ceramic, and a^3=p with p being the porosity content and K_s=1.1 is the aspect ratio. The dielectric response of the porous material is considered here as if the pore had the shape of parallelepiped with square base with side B and height A. In this way, the parameter K_s is defined as A/B.

It should be noted that the dielectric measurements are extremely sensitive to low volume percent phases with low dielectric permittivity in series with high dielectric permittivity materials.

By considering the above microstructure analysis in the light of the dielectric response at 1 kHz a better understanding of the microstructural connectivity is provided, that supports the hypothesis of a pore population constituted by the sum of different contributions. In fact the variance (=1.1) and the mean (μ=2.42) of the Birnbaum–Saunders distribution agree with the data obtained with the modified 3–3 model (with open pores) applied on ε_{33c}^T, that assumes an aspect ratio of 2. On the other hand, the aspect ratio

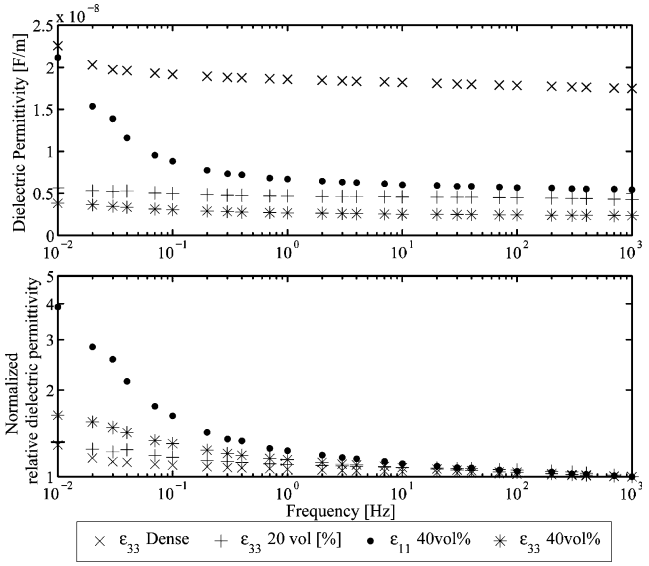

Fig. 5 Low frequency dielectric spectroscopy measurement

(=1.1) obtained by applying the modified cube model to the ε^{T}_{11c} response, differs substantially from the mean obtained with image analysis. The main effect on the dielectric constant arises from the low volume percent of medium-sized pores, that are assumed to have an high aspect ratio. In this perspective, when ε^{T}_{33c} is measured, the medium-sized pores are aligned perpendicularly to the applied electric field and their contribution is high; their influence is low on ε^{T}_{11c} and the final dielectric properties are well approximated by a cubic model.

3.3 Low frequency dielectric spectroscopy

At frequencies lower than 100 Hz, the dielectric behaviour of the porous material differs significantly from that at

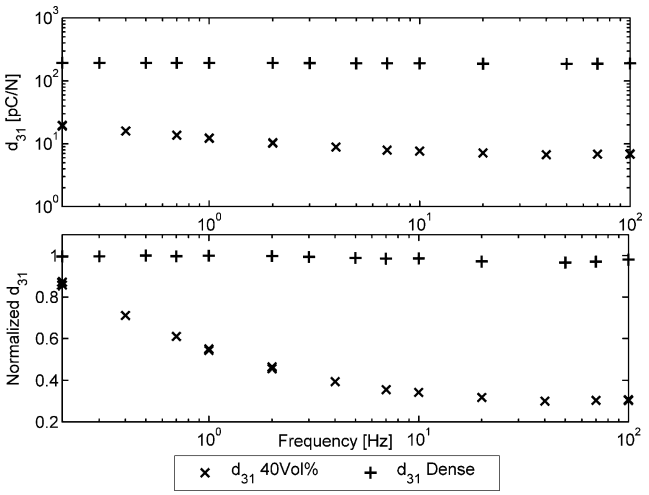

Fig. 6 Low frequency piezoelectric properties measurement

Table 1 Comparison of the d_{31} and d_{33} measured at resonance (100 kHz) and 250 Hz respectively, for samples with different porosity content.

Porosity %	d_{31} [10^{-12} m/V]	d_{33} [10^{-12} m/V]
2.1	−216.16	482
5.4	−179.10	396
20.2	−51.08	312
38.2	−14.64	202

1 kHz as shown in Fig. 5. As reported elsewhere [32], the dielectric permittivity and piezoelectric coefficients of dense PZT materials exhibit logarithmic or power law dependence on the driving field frequency. Experimentally, the dielectric permittivity of the porous material moves away from that behaviour as the pore content increases. The most likely origin of this discrepancy is probably related to a Maxwell–Wagner mechanism often observed in multi-phase materials [33]. Since air is an insulator at low fields, it is unlikely that it contributes to the Maxwell–Wagner behaviour. A better explanation could be attributed to the presence of defects or adsorbed atmospheric humidity on the surface of the pores. For example, reaction of graphite with ceramics could lead to reduction of the ceramics and high concentration of oxygen vacancies at the pores/ceramics interface. From the fabrication process of RAINBOW ceramics [34], it is known that reduction can be so strong as to produce a metallic layer at the graphite/PZT interface. In this perspective the surface of the pores can act as paths with higher conductivity and, depending on the pore morphology and distribution, induce different relaxa-

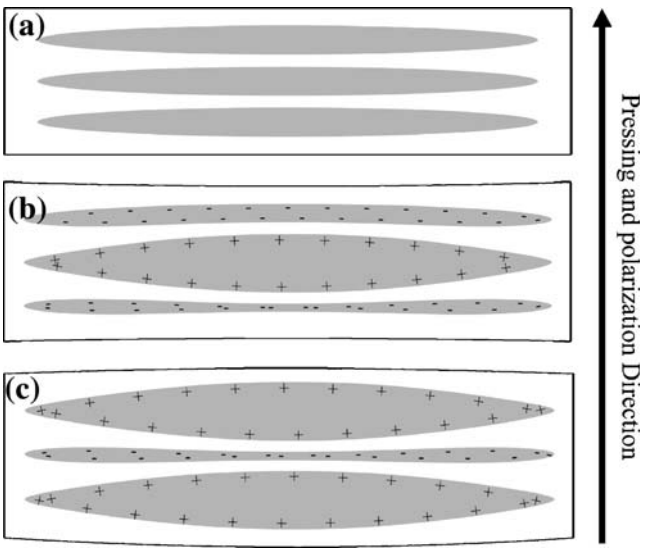

Fig. 7 Outline of the vibration of the porous material subjected to transverse force (**a**) The transverse force is 0 (the sample is at rest) (**b**), (**c**) the sample is subjected to tensile stress. The bending displacement of the walls induce random charges with average tending to vanish

tion time. If this approach is valid, the relaxation time expected for the material with 40 vol. % of porosity is $\tau > 100s$. Apart from differences in the connectivity, the dielectric relaxation of porous ceramics with conductive pore/ceramic interface would have a similar physical origin as the well-known dielectric relaxation in barrier layer capacitors [34].

3.4 Dynamic stress measurements

The behaviour of the piezoelectric constant d_{31} at low frequency is consistent with the trend of the dielectric permittivity (Fig. 6). As the porosity content increases, the value of the piezoelectric constant becomes more sensitive to the frequency. In fact, it is observed that it is approximately constant for the dense material, in agreement with the logarithmic or power law frequency dependence of the properties of ferroelectrics, invoked in the previous section. On the other hand, the sample with 40 vol.% porosity content shows a marked increase of the piezoelectric constant as the frequency decreases. This behaviour is again consistent with Maxwell–Wagner relaxation for the piezoelectric effect that has been observed in other piezoelectric ceramics containing two or more phases or anisotropic grains [35] and polymer-ceramics composites [31]. In the simple bilayer serial model described in Ref. [35] it is shown that the Maxwell–Wagner type piezoelectric relaxation appears in composites whenever two phases have different piezoelectric coefficients and conductivities (in one of the phases, the piezoelectric effect can be zero).

In the direct piezoelectric effect, one or both phases are polarized by external driving pressure. The piezoelectric charges accumulate at the interfaces between the two phases creating depolarizing electric fields within each phase. If the conductivities of the two phases are nonzero and different, the piezoelectric charge will drift with time leading to the time dependent piezoelectric response of the composite and apparent frequency dependence of the piezoelectric coefficient. In our case, the role of the non piezoelectric phase with a higher conductivity is possibly played by pores with conducting ceramic/pore interface. As described by Turik et al., [36] such a composite would produce relaxation not only in d_{33} but also in d_{31}, and ε_{33}. Clearly, the conduction path and efficiency of the piezoelectric charge decay at interfaces depends on geometry and relative volume of the phases. The relaxation in porous ceramics is stronger in d_{31} than in d_{33} [15]. The faster decay of d_{31} (in comparison to d_{33}) for the sample with anisotropic porosity (Table 1) than in the sample with isotropic porosity [37], makes it clear that it can be attributed to the pores anisotropy (pores aligned perpendicular to the direction of applied pressure). As discussed previously, the microstructure developed by using graphite as pore forming agent is anisotropic with pores and voids lengthened in direction 1 perpendicular to applied pressure during sample pressing and during piezoelectric measurements). For the isotropic porosity, the enhanced relaxation of d_{31} over d_{33} (at increasing pore volume) could be due to the fact that a transverse force (in the direction 1) induces a longitudinal deformation (along direction 3) of the pore walls leading to higher effective field responsible for the relaxation [32]. The readers interested in more details on anisotropic relaxation of piezoelectric properties in composites with particles with different aspect ratio are referred to theoretical paper by Turik et al. [36]. In our case, the presence of anisotropic porosity with long and thin walls between adjacent pores (Fig. 7), enhances this effect further increasing the effective d_{31} at lower frequencies.

4 Conclusions

Porous materials with high anisotropic porosity were manufactured and characterized. A semi quantitative study of the microstructure was performed with analysis of SEM images and of dielectric permittivity. The morphology of the pores was related with the enhancement of the piezoelectric coefficient d_{31} at frequencies below 1 Hz, in comparison with the same amount of isotropic porosity. The explanation proposed for this behaviour is the enhanced pore wall deformation in the direction perpendicular to applied transverse stress.

Acknowledgements The authors sincerely acknowledge Mr. C. Capiani for the skillful preparation of samples and Dr. S. Guicciardi, Dr. D. Sciti and Dr. C. Zanelli for the fruitful discussions.

References

1. N. Setter, Piezoelectric materials in devices, ed. by N. Setter (2002)
2. K. Mizumura, Y. Kurihara, H. Ohashi, Jpn. J. Appl. Phys **32**, 2282 (1993). doi:10.1143/JJAP.32.2282
3. H. Kara, R. Ramesh, R. Stevens, C.R. Bowen, IEEE T. Ultrason. Ferr **50**, 289 (2003). doi:10.1109/TUFFC.2003.1193622
4. R. Ramesh, H. Kara, C.R. Bowen, Comput. Mater. Sci **30**, 397 (2004). doi:10.1016/j.commatsci.2004.02.027
5. Q.M. Zhang, H. Wang, J. Zhao, J.T. Fielding, R.E. Newnham, L. E. Cross, IEEE T. Ultrason. Ferr **43**, 36 (1996). doi:10.1109/58.484461
6. T.E. Gomez, M.F. Montero de Espinosa, L.F. Levassort, M. Lethiecq, A. James, E. Ringgard, C.E. Millar, P. Hawkins, Ultrasonics **36**, 907 (1998)
7. R.E. Newnham, D.P. Skinner, L.E. Cross, Mater. Res. Bull. (Sun Chiwawitthaya thang Thale Phuket) **13**, 525 (1978)
8. E.K. Akdogan, M. A llahverdi. A. Safari IEEE T. Ultrason. Ferr. **52**, 746 (2005). doi:10.1109/TUFFC.2005.1503962
9. E. Roncari, C. Galassi, F. Craciun, C. Capiani, A. Piancastelli, J. Eur. Ceram. Soc **21**, 409 (2001). doi:10.1016/S0955-2219(00)00208-9

10. A. Stancu, L. Mitoseriu, L. Stoleriu, D. Piazza, C. Galassi, D. Ricinschi et al., Physica B **372**, 226 (2006). doi:10.1016/j.physb.2005.10.054
11. I. Rychetsky, J. Petzelt, T. Ostapchuk, Appl. Phys. Lett **81**, 4224 (2002)
12. Z. He, J. Ma, R. Zhang, Ceram. Int **30**, 1353 (2004)
13. D. Sciti, S. Guicciardi, A. Bellosi, J. Eur. Ceram. Soc **21**(5), 621 (2001). doi:10.1016/S0955-2219(00)00254-5
14. A. Barzegar, D. Damjanovic, N. Setter, IEEE Trans. UFFC **51**, 262 (2004)
15. D. Piazza, C. Capiani, C. Galassi, J. Eur. Ceram. Soc **25**, 3075 (2005). doi:10.1016/j.jeurceramsoc.2005.03.193
16. J.A. Díaz-García, V. Leiva-Sánchez, J. Stat. Plan. Infer. **128**, 445 (2005) and erratum 137, 1512 (2007)
17. H. Banno, Jpn. J. Appl. Phys **32**, 4214 (1993). doi:10.1143/JJAP.32.4214
18. D.P. Almond, C.R. Bowen, Phys. Rev. B **92**, 157601 (2004)
19. F. Levassort, M. Lethiecq, IEEE T. Ultrason. Ferr **46**, 1028 (1999). doi:10.1109/58.775670
20. Q.Y. Jiang, L.E. Cross, J. Mater. Sci **28**, 4536 (1993). doi:10.1007/BF01154968
21. F. Craciun, G. Guidarelli, C. Galassi, E. Roncari, Ultrasonics **36**, 427 (1998)
22. R.W. Rice, Key Eng. Mater **115**, 1 (1996)
23. K. Darcovich, L. Bera, K. Shinagawa, Mat. Sci. Eng. A-Struct **341**, 247 (2003)
24. H. Hsiang, F. Yen, C. Huang, Jpn. J. Appl. Phys **34**, 1922 (1995). doi:10.1143/JJAP.34.1922
25. R.W. Rice, Porosity of Ceramics (Marcel Dekker, Inc.) 1998
26. B.O. Aduda, A.R. Boccaccini, Brit. Ceram. T **102**, 103 (2003). doi:10.1179/096797803225001641
27. V.Y. Topolov, S.V. Glushanin, J. Phys. D Appl. Phys **35**, 2008 (2002). doi:10.1088/0022-3727/35/16/315
28. A. Wanner, Mat. Sci. Eng. A-Struct **248**, 35 (1998)
29. C.R. Bowen, A. Perry, H. Kara, S.W. Mahon, J. Eur. Ceram. Soc **21**, 1463 (2001). doi:10.1016/S0955-2219(01)00042-5
30. H. Banno, Jpn. J. Appl. Phys **33**, 5518 (1994). doi:10.1143/JJAP.33.5518
31. H. Banno, Am. Ceram. Soc Bull **66**, 1332 (1987)
32. D. Damjanovic, S.S.N. Bharadwaja, N. Setter, Mat. Sci. Eng. B-Solid **120**, 170 (2005)
33. A.R. Von Hippel, *Dielectrics and Waves* (MIT Press, Cambridge, MA, 1954)
34. A.J. Moulson, J.M. Herbert, *Electroceramics—Materials, Properties, Applications* (Chapman and Hall, London, 1990)
35. D. Damjanovic, M. Demartin Maeder, P. Duran Martin, C. Voisard, N. Setter, J. Appl. Phys **90**, 5708 (2001). doi:10.1063/1.1412272
36. A.V. Turik, A.I. Chernobabov, G.S. Radchenko, S.A. Turik, Phys. Solid State **46**, 2213 (2004). doi:10.1134/1.1841382
37. G. Gaillard-Groleas, M. Lagier, D. Sornette, Phys. Rev. Lett **64**, 1577 (1990). doi:10.1103/PhysRevLett.64.1577